

Synthesis and Electrochemical Properties of Mesoporous SnO₂/C Composites as Anode Materials for Lithium Ion Batteries

Guang-Yin Liu, Hui-Yuan Wang*, Bo Jin, Zhi-Zheng Yang, Wen Qi, Yu-Chang Liu, Qi-Chuan Jiang*

Key Laboratory of Automobile Materials of Ministry of Education & School of Materials Science and Engineering, Jilin University, Changchun 130025, China

*E-mail: wanghuiyuan@jlu.edu.cn; jiangqc@jlu.edu.cn

Received: 30 January 2013 / Accepted: 28 February 2013 / Published: 1 April 2013

Mesoporous SnO₂/C composites are prepared by a facile microemulsion method at ambient temperature followed by calcination under N₂ at 600 °C for 2 h. The microstructure and morphology of the samples were characterized by X-ray diffraction, field emission scanning electron microscopy and transmission electron microscope. Galvanostatic discharge/charge tests, cyclic voltammetry and electrochemical impedance spectroscopy were used to characterize their electrochemical properties. It is demonstrated that the SnO₂/C composites exhibit good electrochemical performance. After 50 discharge/charge cycles, they are able to deliver a capacity of 571 mAh·g⁻¹ at a current density of 100 mA·g⁻¹, which is two times greater than that of bare SnO₂ nanoparticles. Such enhanced Li-ion intercalation performance can be attributed to the composites consisting of nanoparticles with fine crystalline size of around 5 nm compared with bare SnO₂ nanoparticles with about 15 nm, the carbon nano-coating increasing electronic conductivity and the mesoporous structure of the composites.

Keywords: Lithium-ion batteries; Microemulsion method; Anode materials; SnO₂

1. INTRODUCTION

Lithium-ion batteries (LIBs) have been used as the power source for most portable electronic devices and are promising energy-storage candidates for electric vehicles [1-2]. Usually, graphite or carbon materials are chosen as anode for commercial LIBs, however, their theoretical capacities are insufficient to satisfy the increasing demand of power density for LIBs. To improve the energy density of LIBs, much research has been attempted to explore new electrode materials or design novel nanostructure of electrode materials [3-8]. With the theoretical reversible capacity of 782 mAh·g⁻¹ and

low discharge potential, SnO₂-based materials have attracted a lot of attention and are regarded as one of the most promising anode candidates for LIBs [6, 9].

However, similar to other alloy-type anode materials, the application of SnO₂ is limited by the poor cyclic performance owing to the pulverization and subsequent electrical disconnection of the electrode caused by extremely large volume change (up to about 300%) during the insertion and extraction processes of Li⁺ [10-11]. Recently, substantial efforts have been made to minimize such a huge volume change, including morphology and composition controls of anode materials [5-13]. One strategy is to design the nanostructure of electrode materials. Especially, the hollow or porous nanostructures exhibit enhanced cyclability because the local empty space in structures can partially hinder its volume expansion [5, 12-13]. However, the active surfaces of nanostructured SnO₂ decrease its coulombic efficiency and the hollow structure would collapse after cycling [14-15]. Another commonly used strategy is to fabricate composite with other materials, which can restrain the volume change of SnO₂ during cycling [16-25]. In particular, nano-painting with carbon has recently been found simple and effective for improving cyclability. For example, Lou and co-workers [26] reported hollow SnO₂/C composites exhibiting a capacity of 460 mAh·g⁻¹ after 100 cycles at a current density of 500 mA·g⁻¹. Carbon is believed to play several important roles upon cycling. First, carbon functions as a physical buffering layer that cushions the stress induced by volume expansion/contraction (cushion effect) [16-17]. Second, its elastic nature makes it very effective to accommodate the volume expansion [17-21]. Third, carbon itself is anode material and can increase the electronic conductivity of the composite electrode [16].

In this study, we prepared uniform SnO₂/C composites by a simple microemulsion process. As-prepared SnO₂/C composites were tested as an anode material for LIBs, which exhibit high reversible capacity and good cycling performance, indicating their promising applications as anode materials for rechargeable LIBs.

2. EXPERIMENTAL

2.1 Materials synthesis

Analytical grade SnCl₄·5H₂O, glucose, n-pentanol, cyclohexane, hydrazine hydrate and cetyltrimethylammonium bromide (CTAB) were used as received without further purification. In a typical synthesis of SnO₂/C composites, two identical solutions were separately prepared by dissolving CTAB (0.5g) in 10 mL of cyclohexane and 2.5 mL n-pentanol. The mixing solution was stirred for 10 min. Then, 4.5 mL of 5 mmol SnCl₄·5H₂O and 2.0 mL of 0.5 mmol of glucose (SnCl₄·5H₂O:glucose molar ratio of 10:1) aqueous solutions were added to the two solutions, respectively. After vigorous stirring at room temperature for 10 min, the two solutions were mixed rapidly and 4 mL hydrazine hydrate was added dropwise into the mixture, continued to stir for 30 min. and set aside at room temperature for 24 h. Finally, a white precipitate was formed, and washed with deionized water and absolute ethanol for several times, and then dried in vacuum at 60 °C for 12 h. At last, the powders were heated at 600 °C for 2 h under ultra high purity N₂. For comparison, bare SnO₂ nanoparticles

were prepared through the same process in the absence of glucose and the received powders were heated at 600 °C for 2 h in air.

2.2 Materials characterization

The synthesized products were characterized by powder X-ray diffraction (XRD, Rigaku-D/Max 2500PC/Japan, using Cu K α radiation, $\lambda=1.5406$ Å), field emission scanning electron microscopy (FESEM, FEIXL-30/USA), transmission electron microscopy (TEM, FEI-TECNAI G2 F20/USA, operating at an accelerating voltage of 200 kV). Brunauer-Emmett-Teller (BET) surface area and pore volume were estimated using ASAP 2420 (USA). Elemental analysis (EA) was performed for carbon with a Flash EA 1112 elemental analysis system (USA).

2.3 Electrochemical measurements

The products were mixed with acetylene black and polyvinylidene fluoride (PVDF) which was resolved in N-methyl-2-pyrrolidone at a weight ratio of 40:40:20. The slurry was uniformly pasted on Cu foil. The prepared electrodes were dried at 120 °C for 12 h in a vacuum oven. The CR2025-type half-coin cells were assembled in an argon-filled glove box with H₂O and O₂ contents below 1 ppm. Metallic lithium foil was used as the counter and reference electrode. The electrolyte consists of a solution of 1 M LiPF₆ in mixture of ethylene carbonate (EC), and dimethyl carbonate (DMC) ethyl methyl carbonate (EMC) with an EC:DMC:EMC volume ratio of 1:1:1. Charge-discharge performances were evaluated by a LAND CT2001A battery instrument at a constant current density in the voltage range of 0.05-3.0V at room temperature. Cyclic voltammetry (CV) measurements were carried out on a CHI650D electrochemical workstation over the potential range 0.05-3.0 V vs. Li/Li⁺ at a scanning rate of 0.1 mVs⁻¹. Electrochemical impedance spectroscopy (EIS) measurement was carried out by applying an AC voltage of 5 mV over the frequency range from 0.01 Hz to 100 kHz.

3. RESULTS AND DISCUSSION

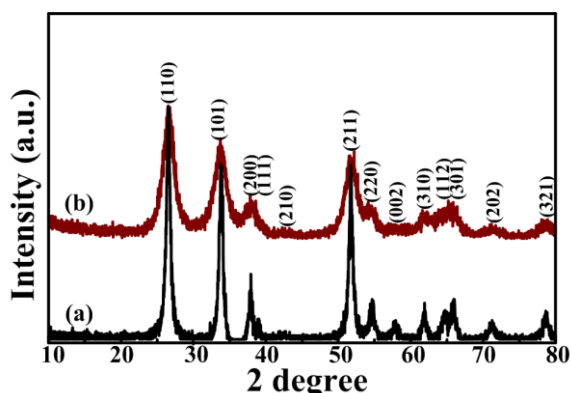


Figure 1. XRD patterns of the (a) bare SnO₂ and (b) SnO₂/C composites.

Crystal structures of as-prepared bare SnO_2 and SnO_2/C composites are inspected by XRD, and shown in Fig. 1a and b, respectively. The characteristic diffraction peaks can be assigned to the tetragonal SnO_2 (JCPDS No. 41-1445). No significant peak of carbon is observed in SnO_2/C composites because of its low content and amorphous state (Fig. 1b). The broad XRD peaks of SnO_2/C composites demonstrate that they have smaller crystallite dimensions than bare SnO_2 due to the inhibition of crystal growth in the presence of carbon generated from glucose [16, 28-30]. The average crystalline sizes calculated by Scherer's formula from (110), (101) and (211) planes are ~ 14 and ~ 5 nm for bare SnO_2 and SnO_2/C composites, respectively.

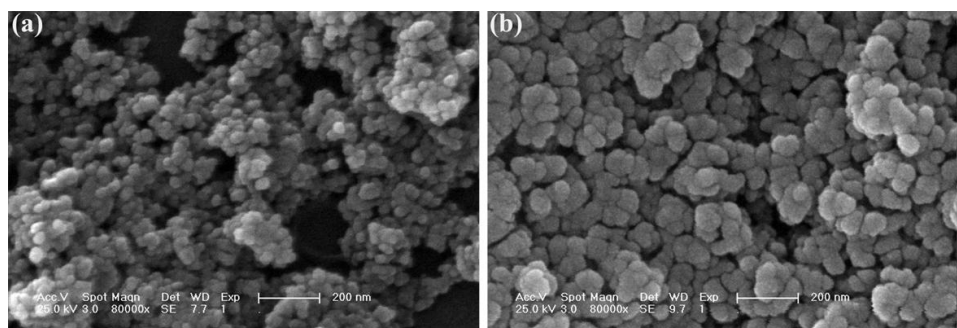


Figure 2. FESEM images of the (a) bare SnO_2 and (b) SnO_2/C composites.

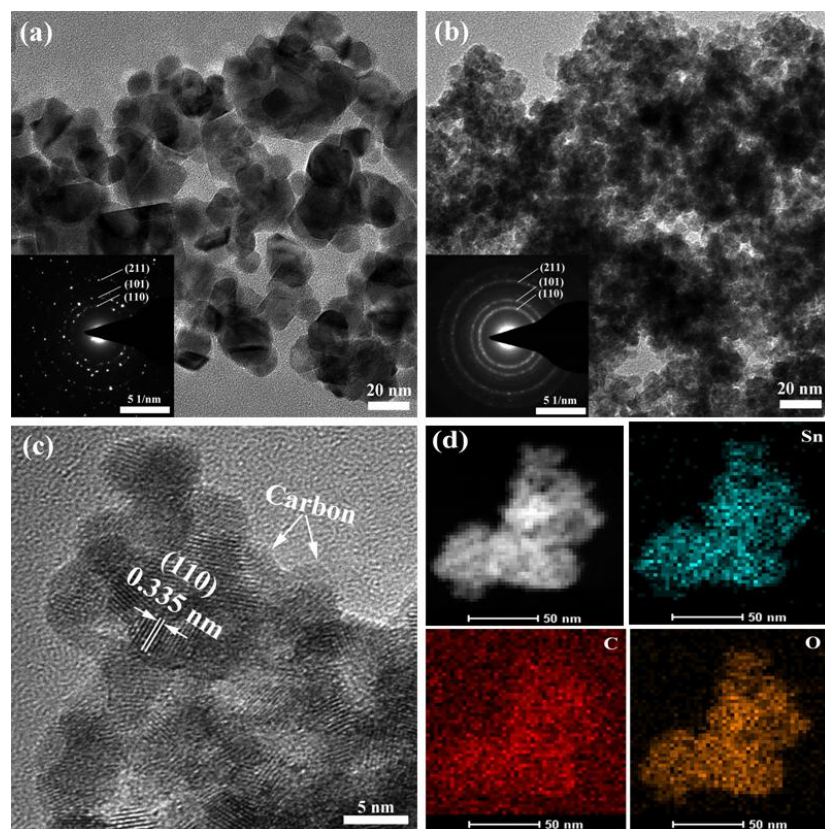


Figure 3. TEM images of the (a) bare SnO_2 and (b) SnO_2/C composites, as well as the (c) HRTEM images and (d) Element mappings of Sn, C and O for SnO_2/C composites.

Figure 2a and b display typical FESEM images of bare SnO_2 and SnO_2/C composites, respectively. The SnO_2 nanoparticles can be clearly seen from Fig. 2a. However, SnO_2/C composites exhibit submicrospherical morphology with a highly rough surface and average particle size of around 100 nm (Fig. 2b) after mixed with glucose. Seemingly, the SnO_2/C composites are composed of small crystallites.

To explore its inherent structures, bare SnO_2 and SnO_2/C composites are further characterized by TEM, as shown in Fig. 3. From TEM images (Fig. 3a), it can be seen that the particle size of bare SnO_2 is less than ~ 20 nm. The corresponding selected-area electron diffraction (SAED) pattern (inset of Fig. 3a) indicates typical diffraction ring for the tetragonal SnO_2 . However, Fig. 3b clearly demonstrates disordered wormhole-like mesoporous pore for SnO_2/C composites. The corresponding SAED pattern (inset of Fig. 3b) indicates that the composites are fine polycrystallines and diffraction rings can be indexed to the (110), (101) and (211) planes, coinciding with tetragonal SnO_2 . Besides, the HRTEM (Fig. 3c) obviously reveals that the crystalline size is ~ 5 nm for SnO_2/C composites, which is consistent with the result calculated by Scherer's formula. The lattice fringes with an interplanar distance of 0.335 nm corresponds to the d-spacing of the (110) crystal plane of SnO_2 . Moreover, it is clearly indicated that the thin carbon layer with a thickness of around 1 nm is coated on the surface of SnO_2 nanoparticles (Fig. 3c). The C content was determined by elemental analysis, indicating that the amount of C is about 4.2 wt.% in SnO_2/C composites. In addition, the evenly distributed carbon-coating layer on nanocrystalline SnO_2 is further demonstrated by the Sn, C and O mappings of SnO_2/C composites (Fig. 3d).

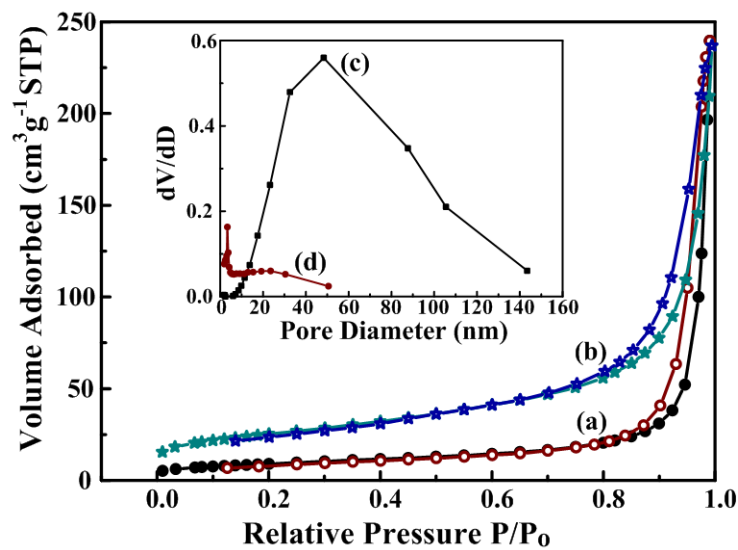


Figure 4. N_2 adsorption/desorption isotherms of the (a) bare SnO_2 and (b) SnO_2/C composites. The inset shows BJH pore-size distributions of the (c) bare SnO_2 and (d) SnO_2/C composites.

The N_2 adsorption/desorption isotherms were employed to investigate specific surface areas of bare SnO_2 and SnO_2/C composites, and the results are shown in Fig. 4. Both samples display a typical type-IV isotherm curve, which are characteristics of mesoporous materials [31-32]. To further analyze

pore structures, pore size distribution curves are investigated through Barrett-Joyner-Halenda (BJH), as presented in insets of Fig. 4. The pore size from bare SnO_2 and SnO_2/C composites center at ca. 48 and 3.3 nm, respectively. The BET specific surface areas of bare SnO_2 and SnO_2/C composites are 32.5 and $88.3 \text{ m}^2 \cdot \text{g}^{-1}$, respectively. The carbon coating suppresses the particle growth, contributing to uniformly agglomerated particles that result in a narrow pore size distribution and large surface areas. Moreover, SnO_2/C composites with mesoporous structure and large surface area lead to multiple advances in the performance of LIBs by providing shorter path lengths for both electron and Li-ion transport. The high electrode/electrolyte contacting area helps to accommodate the strain of the Li-ion insertion/extraction [28, 30].

To investigate the electrochemical performance of SnO_2/C composites as an anode for LIBs, discharge/charge cycles were carried out in the voltage range of 0.05-3.0 V at current density of $100 \text{ mA} \cdot \text{g}^{-1}$. To make a clear comparison, we also present the result of bare SnO_2 nanoparticles prepared by the same procedure under the same electrochemical conditions.

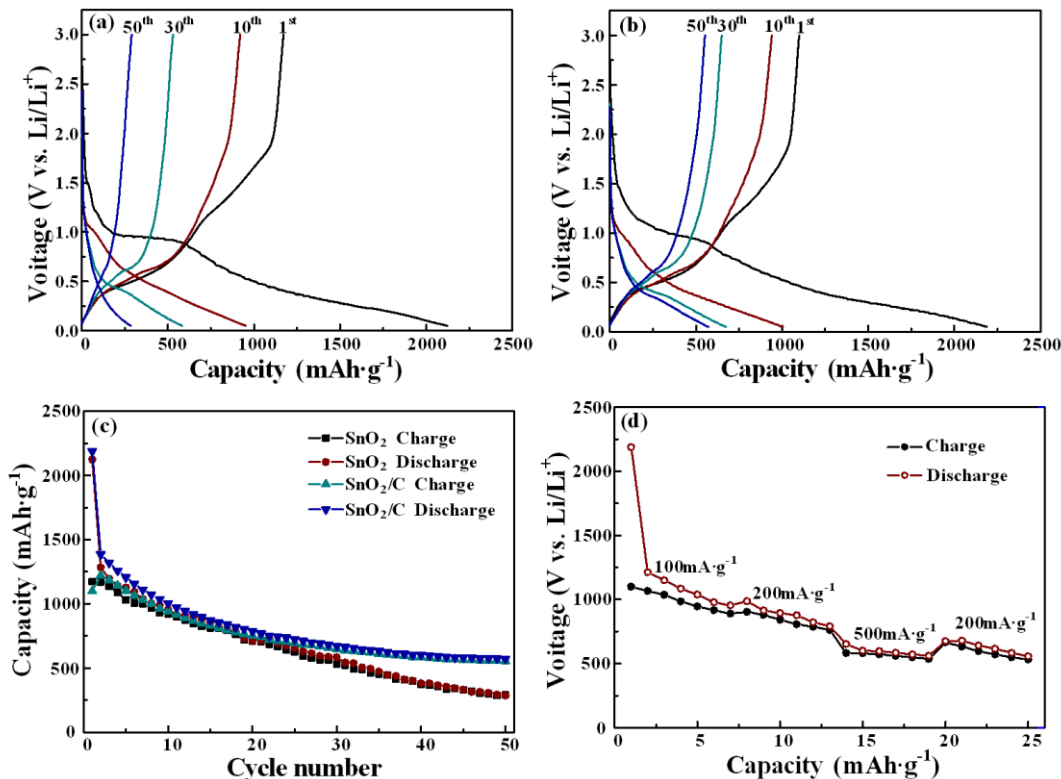


Figure 5. Galvanostatic discharge/charge curves of the (a) bare SnO_2 and (b) SnO_2/C composites, as well as the (c) comparison of the cycling performance of bare SnO_2 and SnO_2/C composites, and (d) rate capacity of SnO_2/C composites.

Figure 5a and b show discharge/charge profiles of bare SnO_2 nanoparticles and SnO_2/C composites in the 1st, 10th, 30th and 50th cycles, respectively. In the first discharge step, both of them present classical plateau at around 0.9 V, followed by sloping curve down to the cutoff voltage of 0.05

V, which is the typical voltage characteristics of SnO_2 -based materials. The first discharge capacities and charge capacities are 2123 and $1171 \text{ mAh}\cdot\text{g}^{-1}$ for bare SnO_2 , and 2188 and $1214 \text{ mAh}\cdot\text{g}^{-1}$ for SnO_2/C composites, respectively. Compared with the theoretical capacity of bulk SnO_2 , the extra discharge capacity is attributed to the formation of a solid electrolyte interphase (SEI) layer generated by an irreversible insertion/deinsertion of Li-ions into host structures or Li alloying reactions and by possible interfacial Li storage [33-35]. Similar phenomena have been observed for metal oxide anodes [17, 35]. The large capacity loss in the first cycle is mainly attributed to the initial irreversible formation of Li_2O , and irreversible lithium loss due to the formation of a SEI layer [25, 36-39]. Obviously, SnO_2/C composites exhibit much better cycling performance than bare SnO_2 (Fig. 5c). It can be seen that the reversible capacity of bare SnO_2 decreases from 1171 at the first cycle to $285 \text{ mAh}\cdot\text{g}^{-1}$ at the 50th cycle. The poor cycling performance of the bare SnO_2 could be attributed to the large volume change during Li^+ insertion/extraction process that causes damage to the structure of SnO_2 nanoparticles. In comparison, the reversible capacity of the SnO_2/C composites retain $571 \text{ mAh}\cdot\text{g}^{-1}$ after 50 cycles, which is twice more than that of bare SnO_2 . The good cyclability in this study can be attributed to two key factors. Firstly, the suitable carbon coating increases the conductivity of the anode material and restrains grain growth of SnO_2 . The small SnO_2 grains reduce the diffusion length and increase the number of active sites for lithium ion insertion/extraction, which is crucial to capacity and cycle performance [25]. Secondly, the carbon serves as a physical buffer, and therefore, SnO_2/C composites can effectively prevent the structural breakdown upon cycling [17-18, 40-42].

To fully estimate the electrochemical performance, the cycling properties at various current densities of 100, 200 and $500 \text{ mA}\cdot\text{g}^{-1}$ are shown in Fig. 5d. The discharge capacity is $985 \text{ mAh}\cdot\text{g}^{-1}$ after 8 cycles at a current density of $100 \text{ mA}\cdot\text{g}^{-1}$, and the discharge capacity over 13 cycles at $200 \text{ mA}\cdot\text{g}^{-1}$ is $792 \text{ mAh}\cdot\text{g}^{-1}$. Even at the high current density of $500 \text{ mA}\cdot\text{g}^{-1}$, it retains high discharge capacity of $561 \text{ mAh}\cdot\text{g}^{-1}$ over 19 cycles. After the current density returns to $200 \text{ mA}\cdot\text{g}^{-1}$, the electrode delivers a capacity of about $557 \text{ mAh}\cdot\text{g}^{-1}$ over 25 cycles. This result suggests that SnO_2/C composites are stable and reversible upon cycling.

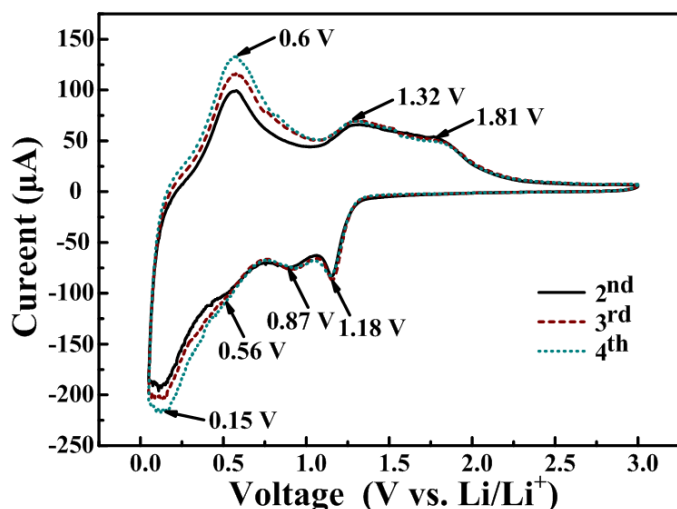


Figure 6. CV curves of the SnO_2/C composites.

To further understand the electrochemical reactions during cycling, CV measurements were performed on SnO₂/C composites, as presented in Fig. 6. They are generally consistent with those in previous studies [43-45]. In the cathodic polarization process, there are two apparent reduction peaks at around 0.87 and 1.18 V, which could be derived from Li₂O formation and electrolyte decomposition (SnO₂+4Li+4e⁻ → Sn+2Li₂O). The other pairs of reduction and oxidation peaks at 0.15 and 0.56 V are related to the formation of Li_xSn phase (Sn+xLi+xe⁻ ↔ Li_xSn (0≤ x ≤4.4)), which are observed to be highly reversible and mainly responsible for the reversible lithium storage capacity in Sn based electrode materials [11, 43]. Meanwhile, in the anodic polarization process, two peaks are recorded at about 0.6 and 1.32 V, and the former represents a de-alloying process of Li⁺ ions (Li_xSn ↔ Sn+xLi+xe⁻ (0≤ x ≤4.4)) [46-47], while the latter is due to the reversible reaction (SnO₂+4Li+4e⁻ → Sn+2Li₂O) [33, 47-48].

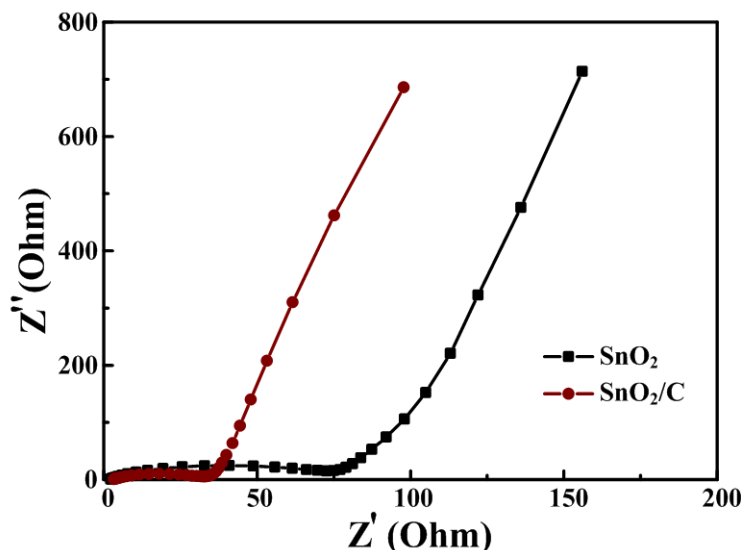


Figure 7. EIS of the bare SnO₂ and SnO₂/C composites.

Figure 7 shows the comparison of EIS between bare SnO₂ and SnO₂/C composites. The EIS results show that each curve consists of a depressed semicircle in the high-middle frequency region and a straight line in the low frequency region. The diameter of the semicircle for SnO₂/C composites is smaller than that of bare SnO₂ electrode, indicating that SnO₂/C composites possess lower contact and charge-transfer resistances. This result suggests that carbon in SnO₂/C composites not only improves the high conductivity of the overall electrode, but also largely enhances the electrochemical activity of SnO₂ nanoparticles during the cycle processes [49].

4. CONCLUSIONS

In summary, we have developed a facile and effective strategy to fabricate mesoporous SnO₂/C composites composed of nanocrystalline SnO₂ and carbon via microemulsion process. The prepared

SnO_2/C composites show better electrochemical performance than the bare SnO_2 with regard to the specific capacity and cycling capability. The improvement of electrochemical performance can be attributed to the tiny SnO_2 nanoparticles, the suitable carbon coating and the abundant mesoporous structure. Therefore, the SnO_2/C composites could be a potential candidate as a high-performance anode for rechargeable LIBs.

ACKNOWLEDGEMENT

This work is supported by The Foundation of Jilin University for Distinguished Young Scholars and Youth Science and Technology Innovation Fund in Jilin University (No. 450060487471).

References

1. M. Armand, J.M. Tarascon, *Nature* 451 (2008) 652-657.
2. G. Du, N. Sharma, V.K. Paterson, J.A. Kimpton, D. Jia, Z. Guo, *Adv. Funct. Mater.* 21 (2011) 3990-3997.
3. Y. Idota, T. Kubota, A. Matsufuji, Y. Maekawa, T. Miyasaka, *Science* 276 (1997) 1395-1397.
4. B. Guo, M. Chi, X.G. Sun, S. Dai, *J. Power Sources* 205 (2012) 495-499.
5. P. Meduri, E. Clark, J.H. Kim, E. Dayalan, G.U. Sumanasekera, M.K. Sunkara, *Nano Lett.* 12 (2012) 1784-1788.
6. C. Wang, Y. Zhou, M. Ge, X. Xu, Z. Zhang, J.Z. Jiang, *J. Am. Chem. Soc.* 132 (2010) 46-47.
7. C.K. Chan, X.F. Zhang, Y. Cui, *Nano Lett.* 8 (2008) 307-309.
8. D.W. Kim, I.S. Hwang, S.J. Kwon, H.Y. Kang, K.S. Park, Y.J. Choi, K.J. Choi, J.G. Park, *Nano Lett.* 7 (2007) 3041-3045.
9. R. Demir-Cakan, Y.S. Hu, M. Autonietti, J. Maier, M.M. Titirici, *Chem. Mater.* 20 (2008) 1227-1229.
10. J.M. Tarascon, M. Armand, *Nature* 414 (2001) 359-367.
11. S. Ding, X.W. Lou, *Nanoscale*. 3 (2011) 3586-3588.
12. X.W. Lou, L.A. Archer, Z. Yang, *Adv. Mater.* 20 (2008) 3987-4019.
13. X.M. Yin, C.C. Li, M. Zhang, Q.Y. Hao, S. Liu, L.B. Chen, T.H. Wang, *J. Phys. Chem. C* 114 (2010) 8084-8088.
14. J.B. Goodenough, Y. Kim, *Chem. Mater.* 22 (2010) 587-603.
15. D. Deng, J.Y. Lee, *Chem. Mater.* 20 (2008) 1841-1846.
16. J.S. Chen, Y.L. Cheah, Y.T. Chen, N. Jayaprakash, S. Madhavi, Y.H. Yang, X.W. Lou, *J. Phys. Chem. C* 113 (2009) 20504-20508.
17. S.M. Paek, E.J. Yoo, I. Honma, *Nano Lett.* 9 (2009) 72-75.
18. F.D. Lupo, C. Gerbaldi, G. Meligrana, S. Bodoardo, N. Penazzi, *Int. J. Electrochem. Sci.* 6 (2011) 3580-3593.
19. X. Yu, S. Yang, B. Zhang, D. Shao, X. Dong, Y. Fang, Z. Li, H. Wang, *J. Mater. Chem.* 21 (2011) 12295-12302.
20. P.C. Lian, X.F. Zhu, S.Z. Liang, Z. Li, W.S. Yang, H.H. Wang, *Electrochim. Acta* 56 (2011) 4532-4539.
21. X.Y. Wang, X.F. Zhou, K. Yao, J.G. Zhang, Z.P. Liu, *Carbon* 49 (2011) 133-139.
22. L. Cui, J. Shen, F. Cheng, Z. Tao, J. Chen, *J. Power Sources* 196 (2011) 2195-2201.
23. H.X. Zhang, C. Feng, Y.C. Zhai, K.L. Jiang, Q.Q. Li, S.S. Fan, *Adv. Mater.* 21 (2009) 2299-2304.
24. J. Xie, S.Y. Liu, X.F. Chen, Y.X. Zheng, W.T. Song, G.S. Cao, T.J. Zhu, X.B. Zhao, *Int. J. Electrochem. Sci.* 6 (2011) 5539-5549.
25. S. Nam, S. Kim, S. Wi, H. Choi, S. Byun, S.M. Choi, S.I. Yoo, K.T. Lee, B. Park, *J. Power*

- Sources 211 (2012) 154-160.
- 26. X.W. Lou, C.M. Li, L.A. Archer, *Adv. Mater.* 21 (2009) 2536-2539.
 - 27. K.T. Lee, Y.S. Jung, S.M. Oh, *J. Am. Chem. Soc.* 125 (2003) 5652.-5653
 - 28. Y.H. Jin, K.M. Min, S.D. Seo, H.W. Shim, D.W. Kim, *J. Phys. Chem. C* 115 (2011) 22062-22067.
 - 29. X.W. Lou, D. Deng, J.Y. Lee, L.A. Archer, *Chem. Mater.* 20 (2008) 6562-6566.
 - 30. L. Shen, C. Yuan, H. Luo, X. Zhang, L. Chen, H. Li, *J. Mater. Chem.* 21 (2011) 14414-14416.
 - 31. A. Vinu, D.P. Sawant, K. Ariga, M. Hartmann, S.B. Halligudi, *Microporous Mesoporous Mater.* 80 (2005) 195-203.
 - 32. K.S.W. Sing, D.H. Everett, R.A.W. Haul, L. Moscou, R.A. Pierotti, J. Rouquerol, T. Siemieniewska, *Pure Appl. Chem.* 57 (1985) 603-619.
 - 33. X.W. Lou, J.S. Chen, P. Chen, L.A. Archer, *Chem. Mater.* 21 (2009) 2868-2874.
 - 34. B. Li, H. Cao, J. Shao, G. Li, M. Qu, G. Yin, *Inorg. Chem.* 50 (2011) 1628-1632.
 - 35. X. Wang, X.L. Wu, Y.G. Guo, Y.T. Zhong, X.Q. Cao, Y. Ma, J.N. Yao, *Adv. Funct. Mater.* 20 (2010) 1680-1686.
 - 36. J. Ye, H. Zhang, R. Yang, X. Li, L. Qi, *Small.* 6 (2010) 296-306.
 - 37. Z. Wang, D. Luan, F. Boey, X.W. Lou, *J. Am. Chem. Soc.* 133 (2011) 4738-4741.
 - 38. X.W. Lou, Y. Wang, C. Yuan, J.Y. Lee, L.A. Archer, *Adv. Mater.* 18 (2006) 2325-2329.
 - 39. G. Derrien, J. Hassoun, S. Panero, B. Scrosati, *Adv. Mater.* 19 (2007) 2336-2340.
 - 40. F. Wang, X. Song, G. Yao, M. Zhao, R. Liu, M. Xu, Z. Sun, *Scripta Materialia.* 66 (2012) 562-565.
 - 41. J. Liu, W. Li, A. Manthiram, *Chem. Commun.* 46 (2010) 1437-1439.
 - 42. W.M. Zhang, J.S. Hu, Y.G. Guo, S.F. Zheng, L.S. Zhong, W.G. Song, L.J. Wan, *Adv. Mater.* 20 (2008) 1160-1165.
 - 43. M.S. Park, G.X. Wang, Y.M. Kang, D. Wexler, S.X. Dou, H.K. Liu, *Angew. Chem. Int. Ed.* 46 (2007) 750-753.
 - 44. M.S. Park, Y.M. Kang, G.X. Wang, S.X. Dou, H.K. Liu, *Adv. Funct. Mater.* 18 (2008) 455-461.
 - 45. Z.H. Wen, Q. Wang, Q. Zhang, J.H. Li, *Adv. Funct. Mater.* 17 (2007) 2772-2778.
 - 46. M. Xu, M. Zhao, F. Wang, W. Guan, S. Yang, X. Song, *Mater. Lett.* 64 (2010) 921-923.
 - 47. P.C. Lian, X.F. Zhu, S.Z. Liang, Z. Li, W.S. Yang, H.H. Wang, *Electrochim. Acta* 56 (2011) 4532-4539.
 - 48. J. Yao, X. Shen, B. Wang, H. Liu, G. Wang, *Electrochim. Commun.* 11 (2009) 1849-1852.
 - 49. J.F. Liang, W. Wei, D. Zhong, Q.L. Yang, L.D. Li, L. Guo, *ACS Appl. Mater. Interfaces.* 1 (2012) 454-459.